Sensing strategies for determining the axial gas dispersion coefficient in bubble columns via gas flow modulation technique

Marchini, S.; Bieberle, A.; Schleicher, E.; Schubert, M.; Hampel, U.;

Originally published:

April 2023

Industrial & Engineering Chemistry Research 62(2023)45, 19225-19237

DOI: https://doi.org/10.1021/acs.iecr.3c00380

Perma-Link to Publication Repository of HZDR:

https://www.hzdr.de/publications/Publ-36713

Sensing strategies for determining the axial gas dispersion coefficient in bubble columns via gas flow modulation technique

Sara Marchini[a*], André Bieberle[b], Eckhard Schleicher[b], Markus Schubert[b,c*], Uwe Hampel[a,b]

[a]Chair of Imaging Techniques in Energy and Process Engineering, Technische Universität Dresden, 01062 Dresden, Germany

[b]Institute of Fluid Dynamics, Helmholtz-Zentrum Dresden-Rossendorf, Bautzner Landstraße 400, 01328 Dresden, Germany

[c]Institute of Process Engineering and Environmental Technology, Technische Universität Dresden, 01062 Dresden, Germany

*Corresponding authors: s.marchini@tu-dresden.de (S. Marchini)

markus.schubert@tu-dresden.de (M. Schubert)

Abstract

The gas flow modulation technique (GFM) is a recently proposed approach for measuring the axial gas dispersion coefficient in bubble columns. It bases on a time-resolved measurement of the modulated gas holdup at different axial positions in the column and a subsequent calculation of the axial dispersion coefficient from amplitude damping and the phase lag of a gas holdup wave. In recent studies holdup has been measured with gamma-ray densitometry, which is advantageous in terms of measurement accuracy. However, the application of radiative measurement techniques in industrial settings poses several logistical and safety challenges. This study investigates the potential of non-radiative measurement techniques in the context of GFM. In particular, differential pressure sensors, conductivity needle probes and optical probes are considered. The results obtained using these alternative techniques are compared with gamma-ray measurements. The comparison qualifies differential pressure sensors as a particular viable alternative to gamma-ray densitometry.

Keywords

Gas flow modulation, axial dispersion coefficient, bubble columns, conductivity needle probes, transmittance optical probes.

HIGHLIGHTS

- Differential pressure sensors are a viable alternative to gamma-ray densitometry for GFM.
- Results obtained using differential pressure sensors are well reproducible.
- Results for optical and conductivity sensors strongly depend on the selected binarization threshold.

1. Introduction

The gas flow modulation technique (GFM) was proposed for the first time by Hampel[1] for the non-invasive experimental investigation of the gas axial dispersion coefficient in bubble columns. The axial gas dispersion coefficient is a fundamental design parameter for bubble column reactors.[2] It is used in the axial dispersion model to account for non-idealities in the gas flow, including recirculation, stagnant areas, axial back-mixing and so on. Contrary to traditional approaches based on tracer substances (e.g., Kantak, et al. [3], Demaria and White [4]), the GFM technique uses a marginal sinusoidal disturbance superimposed on the gas inlet flow rate as virtual tracer. This disturbance introduces a marginal sinusoidal variation of the gas holdup in time, called gas holdup wave. Along the column, the gas holdup wave is damped in amplitude and shifted in phase, due to the gas dispersion. Using a one-dimensional axial dispersion model, Hampel[1] related amplitude damping (V) and phase-shift ($\Delta\phi$) to the value of the axial gas dispersion coefficient as

$$V = \exp\left(\frac{u_{\mathrm{G}}^*}{2D_{\mathrm{G}}}\left[1-\frac{1}{\sqrt{2}}\sqrt{1+\sqrt{1+\frac{16\omega^2 D_{\mathrm{G}}^2}{u_{\mathrm{G}}^{*\,4}}}}\right]\Delta z\right), \qquad 1$$

$$\Delta\phi = -\frac{u_{\mathrm{G}}^*}{D_{\mathrm{G}}\sqrt{8}}\left[\sqrt{\left[\sqrt{1+\frac{16\omega^2 D_{\mathrm{G}}^2}{u_{\mathrm{G}}^{*\,4}}}\right]-1}\right]\Delta z, \qquad 2$$

where D_{G} is the axial gas dispersion coefficient, Δz is the axial distance between the measuring points, u_{G}^* is the bubble rise velocity and ω is the angular modulation frequency. The bubble rise velocity is estimated as $u_{\mathrm{G}}^* = u_{\mathrm{G}}/\bar{\epsilon}$, where u_{G} is the gas superficial velocity and $\bar{\epsilon}$ is the average gas holdup. Recently, Döß et al.[5] experimentally proved the applicability of GFM, while Marchini et al.[6] analysed the inherent uncertainty of the obtained results.

In order to determine the axial gas dispersion coefficient using Equations 1 and 2, the values of the amplitude and phase of the gas holdup wave must be measured at least at two axial positions in the column. For this purpose, Döß et al.[5] used time-resolved gamma-ray densitometry as illustrated in **Figure 1**.

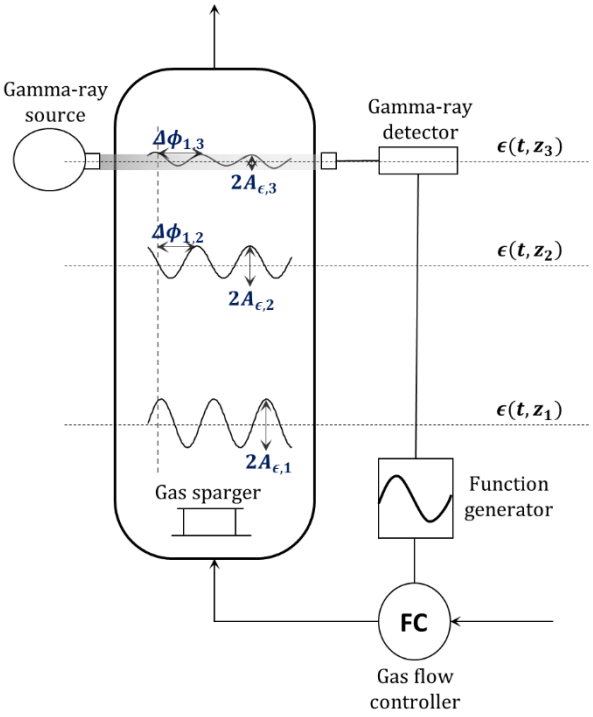

Figure 1. Simplified scheme of the experimental setup for axial gas dispersion measurements using time-resolved gamma-ray densitometry.

Gamma-ray densitometry is based on the linear attenuation of a gamma-photon flux within an object. An isotopic source and a detector are arranged so that the radiation from the source passes the object and is registered by the detector. The attenuation of the radiation depends on the attenuation coefficient of the object material μ according to

$$\langle N\rangle = \langle N_0\rangle \exp(-\mu l), \qquad 3$$

where l is the gamma radiation beam path length in the object and $\langle N_0\rangle$ and $\langle N\rangle$ are the expectation values of the number of gamma photons counted in a given time interval and in absence and presence of the measured object, respectively. In case of a gas-liquid flow, the overall attenuation coefficient is given by

$$\mu_{\mathrm{GL}} = (1-\epsilon)\mu_{\mathrm{L}} + \epsilon\mu_{\mathrm{G}}, \qquad 4$$

where ϵ is the gas holdup. Since $\mu_{\mathrm{G}} \ll \mu_{\mathrm{L}}$, Equation 4 becomes

$$\mu_{\mathrm{GL}} = (1-\epsilon)\mu_{\mathrm{L}}. \qquad 5$$

Considering Equations 3 and 5, the gas holdup can be derived based on the gamma-ray detection events as

$$\epsilon = \frac{1}{\mu_L l} \log\left(\frac{\langle N \rangle}{\langle N_0 \rangle}\right) + 1\,. \qquad 6$$

Radiation-emission-detection processes are subjected to statistical uncertainty, as analysed by Döß et al.[5]. To reduce the impact of the statistics on the measured amplitude and phase, the authors applied a lock-in detection scheme, synchronising the detector data acquisition with the gas flow modulation. The obtained holdup values were, then, ensemble-averaged according to

$$\tilde{\epsilon}_{\mathrm{i}} = \sum_{\mathrm{k}=1}^{n_{\mathrm{p}}} \epsilon_{\mathrm{i}+(k-1)n_{\mathrm{s}}}\,, \quad \text{where j} \in \mathbb{N} \text{ and j} \in [1, n_{\mathrm{s}}] \qquad 7$$

where $\tilde{\epsilon}_i$ is the ensemble-averaged gas holdup in a time interval i, n_{p} is the total number of the modulation periods and n_{s} is the total number of time intervals per modulation period. The ensemble-averaged signal is then fitted by a sine function, from which amplitude and phase of the gas holdup wave are obtained. A scheme explaining this procedure is shown in **Figure 2**. The ensemble-averaging procedure for the gamma-ray densitometry has been outlined by Döß et al.[5]. The authors also motivated the choice of the ensemble-averaging procedure over a Fourier analysis with the presence of a logarithmic transformation in the data processing (see Equation 6). In addition, the ensemble-averaging procedure is advantageous here due to the relatively low data sampling frequency of the gamma-ray densitometry (around 0.1 kHz) and the limited scanning time.

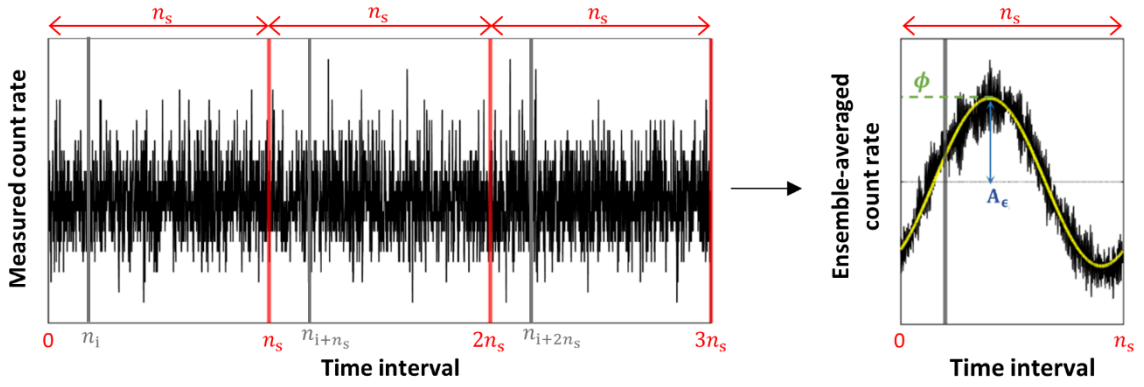

Figure 2. Scheme of the ensemble-averaging procedure applied to a measured gamma ray count rate.

Döß et al.[5] also performed an uncertainty analysis using gamma-ray densitometry for the GFM. According to the authors, this technique has the advantage of being virtually infinitely accurate if a small-sized detector is used and a long measurement time can be realized. However, the radiative nature of this technique limits its applicability in industrial settings. In addition, gamma-ray densitometry systems being able to measure the gas holdup at different axial positions simultaneously are rarely available. In fact, this requires several sources and detectors. Therefore,

measurements are performed at the different axial positions sequentially. This drastically increases the time needed for completing a data set and introduces possible mismatches in the data arising from alterations and drifts in the two-phase flow.

Thus, the present study evaluates the potential of non-radiative and readily available measurement techniques for the GFM. In particular, differential pressure transducers, conductivity needle probes and optical transmission probes are considered.

2. Experimental setup

The experimental setup used in this study is an ID 100 mm bubble column operated with a batch of tap water of 1 m unaerated height. The gas phase was air and its temperature and pressure were monitored. It enters the column through a perforated plate (0.6 mm holes) with 0.18% fractional free area. Before the perforated plate, the gas flow passes a 15 cm high packing of 2 mm glass particles to provide a uniform pressure drop for the gas phase, and thus a more uniform gas distribution through the holes of the perforated plate. The modulation is superimposed on the gas flow using a flow controller (OMEGA FMA2620) with a range from 0 to 20 sL min^{-1} connected to a function generator Agilent 33220A. The accuracy of the gas flow controller is 0.8%. Three axial measurement positions were chosen (located at $z_1 = 125$ mm, $z_2 = 300$ mm and $z_3 = 500$ mm above the gas sparger). At each height position, an optical probe and a conductivity probe were installed with the sensing elements being 30 mm inside of the column. The taps of the differential pressure sensors are 25 mm above and below each measurement height. The three sensors were installed with a circumferential angle of 30° one from another. This configuration left enough free space for performing gamma-ray densitometry measurements. To ensure the comparability of the results, the data from all different measurement techniques were acquired simultaneously. **Figure 3** shows a schematic diagram of the experimental setup.

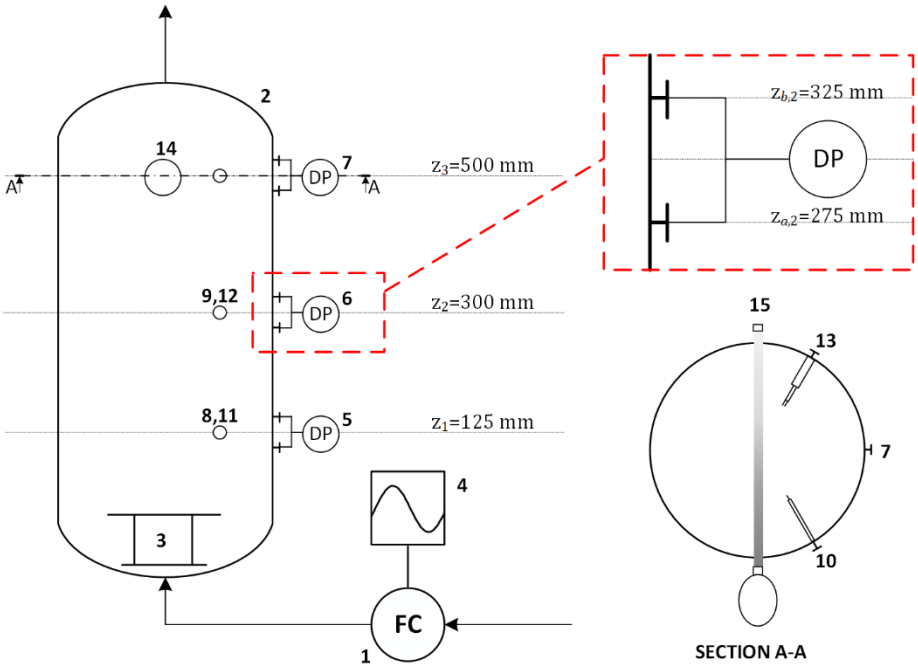

Figure 3. Simplified scheme of the experimental setup and involved measurement techniques (1 – gas flow controller, 2 – bubble column, 3 – gas sparger, 4 – gas flow modulator, 5-6-7 – differential pressure sensors, 8-9-10 – conductivity needle probes, 11-12-13 – optical probes, 14 – gamma-ray source, 15 – gamma-ray detector).

Table 1 reports the details of the applied measurement systems.

Table 1. Design details of the applied measurement techniques.

Gamma-ray densitometry	Custom made; Isotopic source: Cs-137 (662 keV); Detector: scintillator, 8 × 4 mm^2 reception area; Sampling frequency: 100 or 200 Hz.
Differential pressure sensors	OMEGA PXM409; Range: 0-25 mbar; Accuracy: 0.08%; Sampling frequency: 1 kHz.
Conductivity needle sensors	HZDR Innovation GmbH.; Needle diameter: 100 μm; Sampling frequency: 10 kHz.

Optical transmission sensors	Custom made; Light source: red LED (650 nm wavelength); Distance between the fibers: 2.5 mm; Sampling frequency: 1 kHz.

Experiments were performed at different gas flow rates, namely 8 sL min^{-1}, 14 sL min^{-1} and 17 sL min^{-1}. The column was operated at atmospheric pressure. The temperature of the gas outlet flow was monitored during the experiment and was practically constant (18°C). For each flow rate, two different modulation frequencies were applied (0.1 Hz and 0.4 Hz). An initial modulation amplitude of 15 % for the flow rate was applied, as recommended by Marchini et al.[6].

Pressure sensors and optical probes were used at a sampling frequency of 1 kHz. Conductivity needle probes had a sampling frequency of 10 kHz. The frequencies of the gamma-ray detector data read-out were 100 Hz and 200 Hz, for modulation frequencies of 0.1 Hz and 0.4 Hz, respectively. A total scanning time of 3600 s was used for each operating point.

3. Working principles of non-radiative sensing techniques applied to GFM

3.1 Differential pressure sensors

Differential pressure sensors are readily available and inexpensive. Multiple sensors can be easily installed at several axial positions, where the gas holdup wave can be measured simultaneously. Also, differential pressure sensors allow direct holdup estimation without the need for a threshold in data processing.

The gas holdup wave represents a change of the holdup in time at a fixed axial position. Together with the holdup, the hydrostatic pressure changes, too. This change can be written as

$$\frac{\mathrm{d}p(z,t)}{\mathrm{d}z} = \rho_{\mathrm{L}} g \left(1 - \frac{\mathrm{d}z\epsilon(z,t)}{\mathrm{d}z}\right), \qquad 8$$

where p is the local pressure, ρ_{L} is the liquid density and g is the gravitational acceleration. Physically, the term $\left(1 - \frac{\mathrm{d}z\epsilon(z)}{\mathrm{d}z}\right)$ represents a density-corrected hydrostatic height, accounting for the presence of gas. Considering a wet/wet differential pressure sensor with pressure taps at z_a and z_b (see **Figure 3**), the gas holdup can be assumed constant between the pressure taps if $(z_b - z_a)$ is sufficiently small. This gives

$$|\Delta p(t)| = \rho_{\mathrm{L}} g (z_b - z_a)\big(1 - \epsilon(t)\big). \qquad 9$$

After subtracting the initial hydrostatic pressure (i.e. when no gas is flowing), the gas holdup is given by

$$\epsilon(t) = \frac{|\Delta p(t)|}{\rho_{\mathrm{L}} g (z_b - z_a)}. \qquad 10$$

To obtain amplitude and phase of the gas holdup wave using the collected data, two different data processing strategies are possible. The first one relies on the ensemble-averaging procedure as in the case of gamma-ray densitometry. However, this procedure requires some implementation effort and has considerable computational cost in case of large datasets (data sampling frequencies are often >1 kHz). Since only linear transformations are involved in the data processing of the pressure sensor, a Fourier analysis is selected in this study. A fast Fourier transform is applied to the data stream using built-in functions of MATLAB (ver. R2019b). This way, a frequency spectrum and a phase spectrum are obtained. The amplitude spectrum shows a clear peak at the modulation frequency. If the spectrum is normalized with respect to the average holdup, the value of that peak represents the amplitude of the detected gas holdup wave. The peak in the phase spectrum is not immediately clear. This is due to the noise in the signal and to the fact that each frequency that has a non-zero amplitude value in the amplitude spectrum is also associated to a phase. The phase value corresponding to the modulation frequency (where a peak in the amplitude spectrum was identified) is the phase of the gas holdup wave. A detailed description of the applied function and procedure is provided by Viswanathan et al.[7].

Some uncertainties related to differential pressure measurements arise. **Figure 4a** shows an example of predicted signals from three pressure transducers located at different axial positions from the gas sparger (z_1, z_2, z_3 in **Figure 3**). It should be noted that expected differential pressure values are relatively low. Moreover, the amplitude of the expected wave is of the order of a few Pascals only. These conditions are challenging for the measurement system and low-range high-accuracy pressure sensors are strongly recommended. Another source of error in this approach is introduced by the necessary distance between the two taps of each differential pressure sensor located at z_a and z_b. In fact, Equation 3 neglects the change in the gas holdup wave happening between z_a and z_b. This causes a systematic error given by

$$\mathrm{Err}p = \rho_{\mathrm{L}} g \, \epsilon(z,t)|_{\frac{(z_b - z_a)}{2}} - \rho_{\mathrm{L}} g \int_{z_a}^{z_b} \frac{\mathrm{d}\epsilon(z,t)}{\mathrm{d}z} \mathrm{d}z. \qquad 11$$

Considering Equations 1 and 2, the gas holdup wave can be written as a function of the initial modulation characteristics as

$$\epsilon(z,t) = \bar{\epsilon} + A_{\epsilon,0} \exp\left(H_1 \left[1 - \frac{\sqrt{1+H_2}}{\sqrt{2}}\right] z\right) \cos\left(\omega t + \phi_0 - \frac{H_1 \sqrt{H_2 - 1}}{\sqrt{2}} \mathrm{z}\right), \qquad 12$$

where $\bar{\epsilon}$ is the average gas holdup, $A_{\epsilon,0}$ is the product between the initial modulation amplitude and the average gas holdup, ϕ_0 is the initial phase and ω is the angular modulation frequency and H_1 and H_2 are defined as

$$H_1 = \frac{u_{\mathrm{G}}^*}{2D_{\mathrm{G}}} \tag{13}$$

and

$$H_2 = \sqrt{1 + \frac{16\omega^2 D_{\mathrm{G}}^2}{{u_{\mathrm{G}}^*}^4}}. \tag{14}$$

Using Equation 12, Equation 11 becomes

$$\begin{aligned} \frac{1}{A_{\epsilon,0}} \frac{\mathrm{Err}p}{\rho_{\mathrm{L}} g} = {} & \exp\left(K_1 \frac{(z_{\mathrm{b}} - z_{\mathrm{a}})}{2}\right) \cos\left(\omega t + \phi_0 - K_2 \frac{(z_{\mathrm{b}} - z_{\mathrm{a}})}{2}\right) \\ & - \exp(K_1 z_{\mathrm{b}})[K_1 \cos(\omega t + \phi_0 - K_2 z_{\mathrm{b}}) - K_2 \sin(\omega t + \phi_0 - K_2 z_{\mathrm{b}})] \\ & + \exp(K_1 z_{\mathrm{a}})[K_1 \cos(\omega t + \phi_0 - K_2 z_{\mathrm{a}}) - K_2 \sin(\omega t + \phi_0 - K_2 z_{\mathrm{a}})], \end{aligned} \tag{15}$$

where

$$K_1 = H_1 \left[1 - \frac{\sqrt{1 + H_2}}{\sqrt{2}}\right] \tag{16}$$

and

$$K_2 = \frac{H_1 \sqrt{H_2 - 1}}{\sqrt{2}}. \tag{17}$$

Note that Err$p$ is itself a cosine wave of amplitude A_{p} and phase ϕ_{p}. Per its definition, it represents the systematic error introduced when the holdup wave is assumed constant between the taps of the same sensor. A_{p} represents a conservative estimate of the error introduced on the amplitude of the holdup wave. In fact, when summing two sine waves, the total amplitude ranges between the difference and the sum of the single amplitudes. Therefore, the error introduced on the detected amplitude is given by:

$$\mathrm{Err}A_\epsilon = \frac{A_p}{A_\epsilon} \cdot 100. \tag{18}$$

The error on the detected phase (ϕ) can also be estimated based on A_{p} and ϕ_{p} and applying known formula of composition of sine waves. A conservative estimate of this error is obtained assuming a phase shift between the detected pressure wave and Err$p$ equal to $\pi/2$. In this case

$$\mathrm{Err}\phi = \frac{1}{\phi}\left[\phi - \tan^{-1}\left(\frac{A_\epsilon \sin(\phi) + A_p \cos(\phi)}{A_\epsilon \cos(\phi) + A_p \sin(\phi)}\right)\right] \cdot 100 \tag{19}$$

and the introduced error depends only on ϕ, A_ϵ and A_p.

Figure 4b shows the variation of Err$p$ with the distance between the two taps of the same pressure transducer ($z_\mathrm{b} - z_\mathrm{a}$) and for different values of K_1 and K_2.

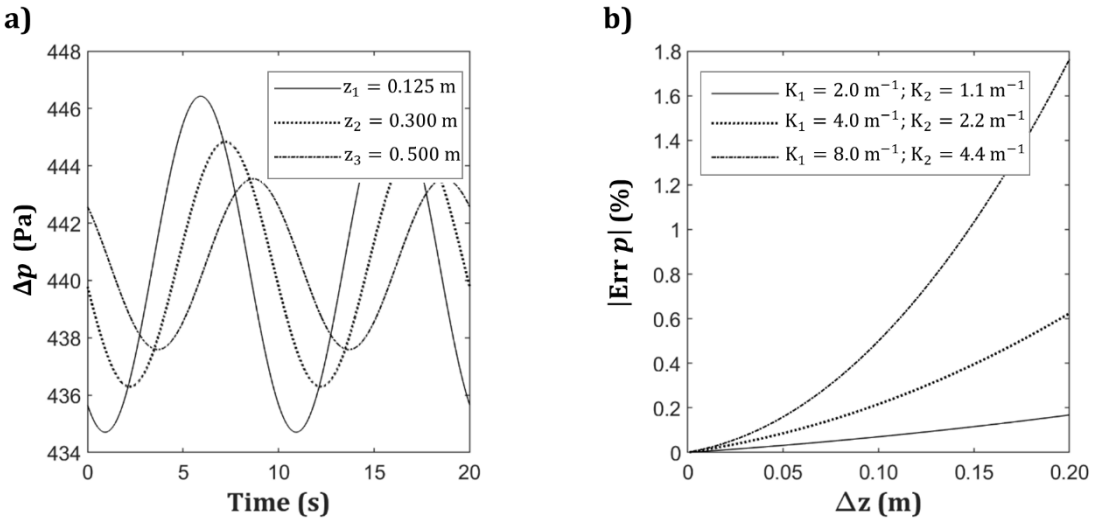

Figure 4. (a) Predicted pressure measurements in time at different axial distances from the sparger ($f = 0.1$ Hz, $D_\mathrm{G} = 0.01\ \mathrm{m^2 s^{-1}}$, $\bar{\epsilon} = 0.10$, $A_\epsilon = 0.015$, $\Delta z = z_\mathrm{b} - z_\mathrm{a} = 0.05$ mm) and (b) predicted error of the pressure measurement for different values of H_1 and H_2 as a function of the axial distance between the taps.

To minimize this error, $\Delta z = z_\mathrm{b} - z_\mathrm{a}$ should be kept as small as possible. However, the accuracy limit and the operating range of the selected pressure transducer must also be taken into account. In fact, the smaller the value of Δz, the lower the measured differential pressure, which increases the impact of the uncertainty.

3.2 Conductivity needle probe

Conductivity probes have often been used to measure phase holdup in gas-liquid contactors (e.g., Munholand and Soucy [8]) with aqueous solution as the liquid medium. For other liquids with low conductivity, capacitance probes can be used. In the case of this study, tap water was used and the term "liquid" will be used in this section referring to tap water.

To perform a measurement, the sensor is positioned inside the column and measures the conductivity of the two-phase flow in time. The conductivity of the continuous phase (liquid) is much higher than the conductivity of the gas bubbles, which practically show no conductivity. Therefore, when a bubble touches the sensor, the measured conductance drastically drops. In this study, a conductivity needle probe was applied. A simplified scheme and a picture are shown in **Figure 5a**.

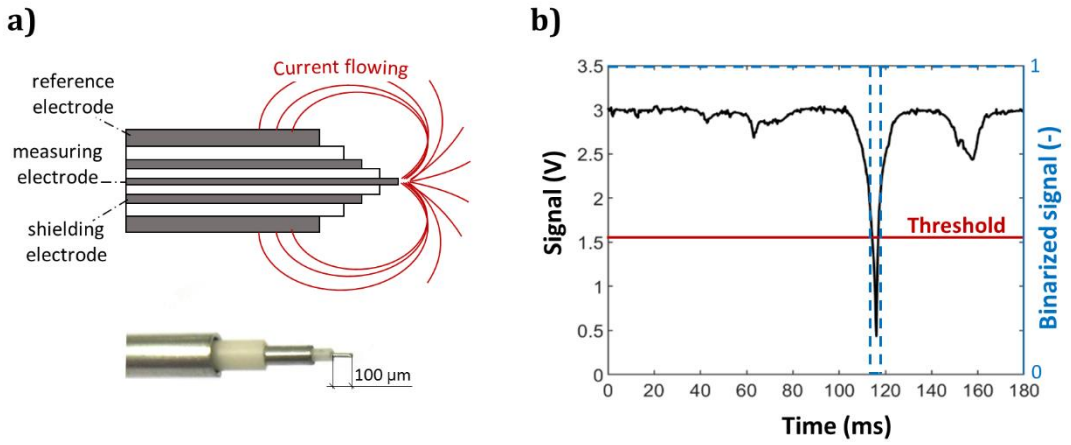

Figure 5. (a) Simplified scheme and picture of the conductivity needle probe and (b) threshold application and processing of conductivity probe signal.

A difference in the potential between the measuring and reference electrodes generates an electrical field around the tip of the probe. To be correctly detected, a gas bubble must be pinched by the measuring electrode (constituted by a needle of 100 µm diameter and length). In this way, the electrical current between reference and measuring electrode is strongly reduced and a dip in the signal is registered (see **Figure 5b)**.

In order to correctly identify single bubbles, the sampling frequency f_d of the sensor must satisfy

$$\frac{1}{f_\mathrm{d}} \ll \frac{d_B}{u_\mathrm{G}^*}, \qquad 20$$

which means that the sampling interval of the sensor is much shorter than the average contact time between a bubble and the sensor. The holdup values are then derived as the ratio between the sum of the contact times of bubbles and sensor and the overall measurement time.

A threshold value is needed to distinguish the bubble contacts from other signal variations. The latter may be due to noise or fluctuations in the liquid conductivity coming from temperature or species concentrations. Another source of local minima in the signal are bubbles passing in the vicinity of the needle, but not being pinched by the latter. As remarked by Dias et al.[9], no established method exists for determining the threshold voltages. Recommended thresholds vary from 10 to 50% of the span between maximum (liquid) and minimum (gas) signal values. In this study, various thresholds were tested and the signals were binarized assigning the value 1 to conductivities above the threshold (liquid phase) and 0 values to conductivities below the threshold (gas phase). **Figure 5b** illustrates the applied procedure.

Again, two data processing strategies are possible. The first strategy is based on ensemble-averaging. In this case, the ensemble-averaged signal undergoes a post-processing step, in which the latter is divided into smaller intervals and each interval is averaged. In this way, support data

points with a better statistics are obtained. These points are, then, fitted to a sinusoid with a least square approach. The second data processing strategy is based on a Fourier analysis performed on the entire binarized signal. This second approach is preferred in this case due to the high sampling frequency >10 kHz provided by the sensors and the absence of logarithmic transformations in the signal processing.

Conductivity needle probes are also readily available and a relatively cheap measurement technique suitable for installation at several axial positions for simultaneous data acquisition. However, the selection of a proper threshold represents a challenge for this approach. **Figure 6** shows the effect of the threshold on amplitude damping and phase-shift. The data were obtained using two conductivity probes at heights z_1 and z_2 for two different operating conditions (Cases 1 and 2).

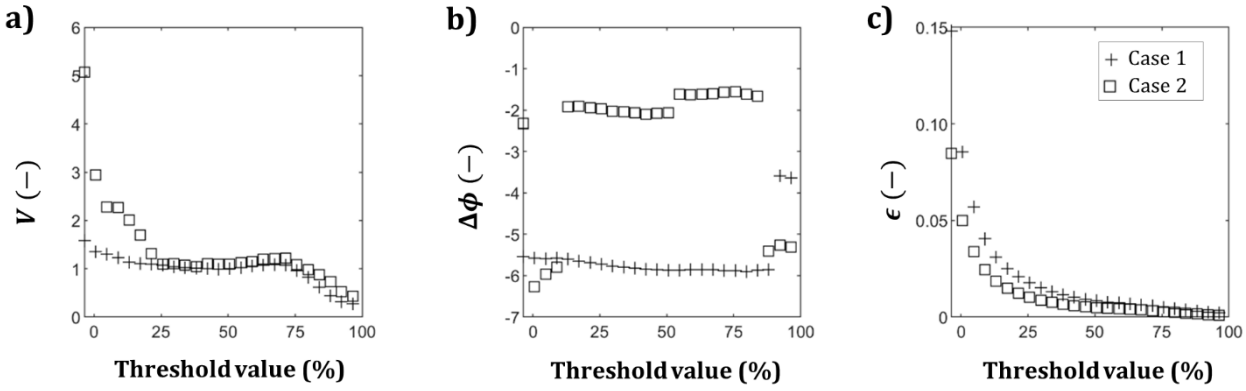

Figure 6. Dependence of extracted (a) amplitude damping, (b) phase-shift and (c) average gas holdup on the threshold value selected for processing of the conductivity needle probe data (Case 1 – gas flow rate 14 sL min^{-1}, modulation frequency 0.1 Hz; Case 2 – gas flow rate 8 sL min^{-1}, modulation frequency 0.4 Hz).

As shown in **Figure 6**, the selected threshold has a non-negligible influence on obtained amplitude damping, phase-shift and average gas holdup. A reasonable criterion for the selected threshold is that the needle probes' measured holdups correspond to those of another threshold-free technique such as pressure sensors. This criterion, however, has some limitations. In fact, holdups obtained via needle probe are highly local and do not necessarily correspond to the holdup measured at other positions in the column cross-section. In addition, the sensor needle might not pinch the bubble properly due to insufficient momentum. In this case, the trajectory of the bubble is simply deviated, and the letter circumvents the needle tip, decreasing the measured gas holdup. **Figure 6a** and **b** show that, while the average holdup value decreases almost exponentially increasing the threshold (**Figure 6c**), amplitude damping and phase-shift remain rather constant for intermediate thresholds. This can be explained as follows. For low threshold values, signal dips not emanating from correctly detected bubbles are wrongly counted and introduce errors in the

calculated amplitudes and phases. For high threshold values, fewer bubbles are counted and the variation of the counted bubbles due to gas flow modulation is too small to be reliably quantified. Intermediate thresholds, instead, allow excluding non-bubble dips, while offering a statistically significant number of bubbles. Intermediate thresholds should, therefore, be preferred when determining amplitude damping and phase-shift. All performed operations in the data processing are linear and amplitude damping and phase-shift are determined using two gas holdup waves subjected to the same threshold. For these reasons, when an appropriate threshold value is selected, amplitude damping and phase-shift do hardly depend on the latter. A 50% threshold was found suitable for all analyzed cases and, therefore, selected in this study. However, the needle probes significantly underestimate the gas holdup, when a 50% threshold is applied. This is because, in this way, only bubbles that are correctly pinched by the needle are counted, while bubbles that only pass in the vicinity of the needle are discarded as non-bubble events. For the reasons explained earlier, only a limited amount of bubbles is correctly pinched and this leads to significant underestimation of the averaged holdup. To obtain reliable measurements of amplitude damping, phase-shift and average gas holdup two different thresholds will be selected in this study. On the one hand, amplitude damping and phase-shift will be evaluated based on a 50% threshold, where their value is fairly independent of the selected threshold value. On the other hand, a suitable threshold will be selected to evaluate the average gas holdup, based on a calibration with differential pressure sensors. In this study, a 5% threshold was used for this purpose. This means however, that conductivity needle probes can only work in combination with another threshold-free measurement technique for determining the average gas holdup. Alternatively, one needs to rely on correlations or previous measurements for the gas holdup value.

For reasons of completeness, the intrusive nature of the needle probes should also be mentioned, which might limit the applicability in industrial environment.

3.3 Optical fiber probes

Transmittance optical fiber probes are commonly applied for measuring gas or solid holdups in (slurry) bubble columns (Dias et al.[9], Schweitzer et al.[10], Xuereb et al.[11]). The working principle of the probe is based on the change of light transmittance between a light emitting fiber and a light receiving fiber during gas bubble contact. Coté et al.[12] have reviewed the different designs of optical fiber probes. For the present study, a double-tip fiber probe with side-firing fibers was used. A picture and a simplified scheme of the applied probe are shown in **Figure 7a**.

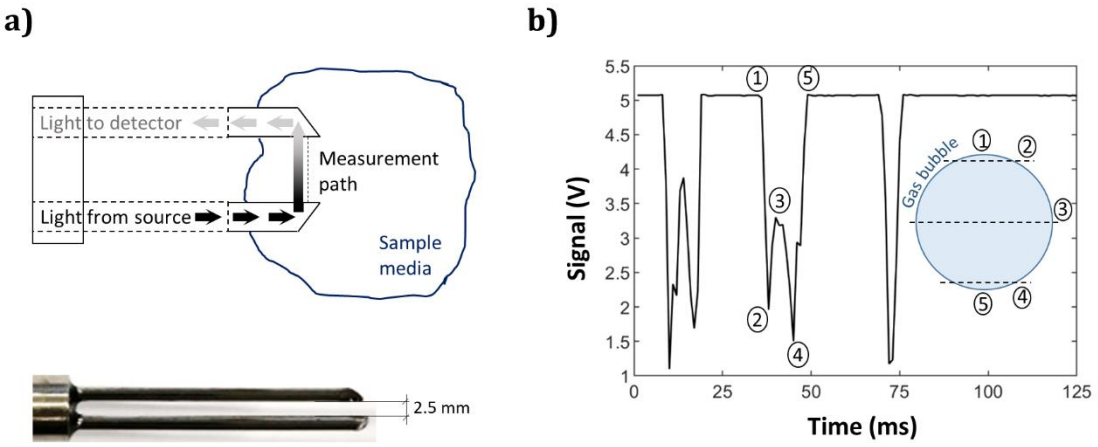

Figure 7. (a) Simplified scheme and picture of a double-tip fiber optical probe and (b) characteristic light power signal of a bubble crossing the measurement path.

Signal reductions indicate the presence of gas bubbles in the measurement plane (**Figure 7b**). When the bubble reaches the proximity of the measurement plane, a part of the light that would be dispersed outside of the measurement path is deflected into the direction of the detector. This causes a slight increase of the light power signal with respect to the ground level (indicated by (1) in **Figure 7b**). When the bubble enters the measurement volume of the probe, a local minimum in the signal is found. This is compatible with the light encountering the bubble surface at its highest curvature and being deflected away from the detector. While the bubble passes, the gas-liquid interface inclination reduces with respect to the fibers and this way progressively more light passes through the bubble, increasing the light power signal (from point (2) to (3) in **Figure 7b**). After the first half of the bubble has passed through the measurement plane, the interface inclination increases again, decreasing the signal (points (3) to (4)). When the bubble exits the measurement plane, the signal increases again until above the base value (point (5)), since a part of the dispersed light is deflected back to the detector.

The data processing procedure is analogue to the conductivity probes. Again, Fourier analysis is preferred over the ensemble-averaging procedure. Also, a threshold value is needed for signal binarization and data processing. The influence of the selected threshold on the detected values of amplitude damping, phase-shift and average holdup value has been investigated and the results are exemplarily reported in **Figure 8** for two operating conditions.

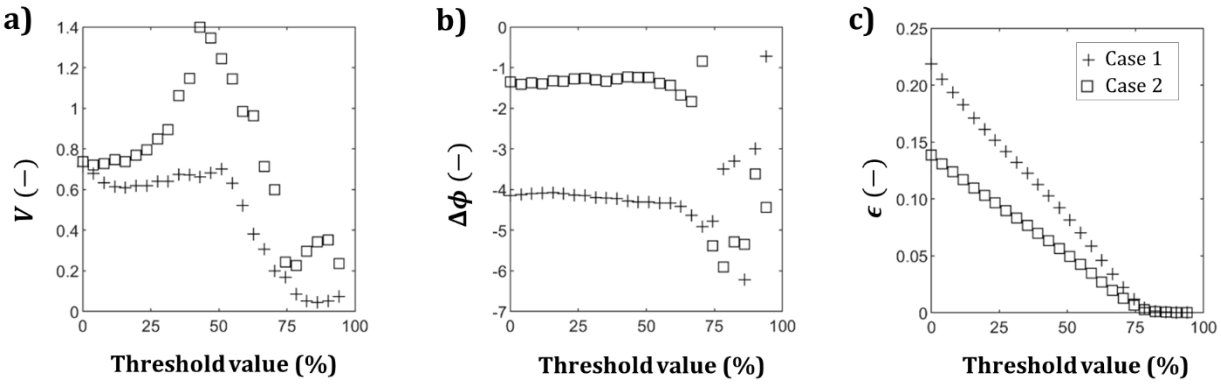

Figure 8. Dependence of extracted amplitude damping, phase-shift and average gas holdup on the threshold value selected for the processing of the optical probe data (Case 1 – gas flow rate 14 sL min^{-1}, modulation frequency 0.1 Hz; Case 2 – gas flow rate 8 sL min^{-1}, modulation frequency 0.4 Hz).

The selected threshold has a strong influence. However, while the holdup decreases almost linearly with increasing threshold value, amplitude damping and phase-shift are relatively constant for low to intermediate thresholds values. The amplitude damping determined for Case 2 shows a peculiar behavior depending on the applied threshold (see **Figure 8a**). In particular, a peak in the amplitude value is registered between 30% and 60% holdup values. Referring to **Figure 7b**, the transition between points 2-3-4 in the signal also happens in this range. If a threshold value in this range is selected, the optical probe wrongly detects two bubbles, instead of a single (larger) one and the gas holdup is altered. The impact of this misdetection on the measured holdup wave depends strongly on how the bubbles pass through the probe and on the bubble characteristics. For example, referring to **Figure 2b**: a larger bubble shifts point 3 in the signal to higher voltage values; a slower bubble extends the time duration of point 3 in the signal. In principle, if all bubbles have the same size, rise at the same velocity and are uniformly distributed, this misdetection affects both probes in the same way. Therefore, one would expect the amplitude values to change, while the amplitude damping remains constant. In practice, however, the measurements performed by the optical probes are highly local and the distance between the light source and detector is in the order of the bubble diameter. On this scale, the hydrodynamic cannot be considered homogeneous. The peak seen in **Figure 8a** Case 2 is most probably related to local hydrodynamic phenomena (such as recirculation) that cause the two probes to systematically detect bubbles of slightly different size and velocity in this particular case. The phase-shift appears less sensitive to this phenomena. This behaviour of the amplitude damping underlines that if the analysis is performed using an incorrect threshold meaningless results are obtained. Specifically for the optical probe, a threshold below 20% should be preferred for the reasons outlined above. Similarly to the conductivity needle probes, for high thresholds only very few bubbles are detected and the amplitudes and phases cannot be determined reliably.

It should be noted that the bubbles are not required to be pinched by the optical probes in order to be detected. Moreover, even if the measurement remains local, the sampling area is much larger than in case of conductivity needle probe. Thus, the considered optical probe is expected to give a reliable estimation of the average gas holdup value. Therefore, it is recommended to select a threshold so that the average gas holdup is consistent with what is measured by pressure sensors at same conditions. In this study, a 10% threshold value was selected (see Section 4.1).

4. Results and discussion

This section summarizes the results of the comparison between differential pressure sensors, conductivity needle probes, transmittance optical probes and gamma-ray densitometry. In particular, average gas holdup, amplitude damping and phase-shift are considered. Eventually, the determined values of the axial gas dispersion coefficient are also reported. Reproducibility of the results has been confirmed for all applied measurement techniques (see **Supplementary Information S2**). The sensor raw data are available at the following DOI: 10.14278/rodare.2152.

4.1 Average gas holdup

Figure 9a shows the average gas holdups measured with the non-radiative techniques ($\bar{\epsilon}^*$) at the three considered measurement planes (z_1, z_2 and z_3) for two modulation frequencies and a total scanning time of 3600 s. These values are compared in the form of a parity plot with the values measured by gamma-ray densitometry ($\bar{\epsilon}_{\mathrm{ref}}$). Threshold values of 5% and 10% have been applied for the data post-processing of the conductivity and optical probes, respectively. **Figure 9b** summarizes the average gas holdup values for all measurement techniques on the three measurement heights as a function of the gas superficial velocity. Reported values are the average of the measurements at the two modulation frequencies.

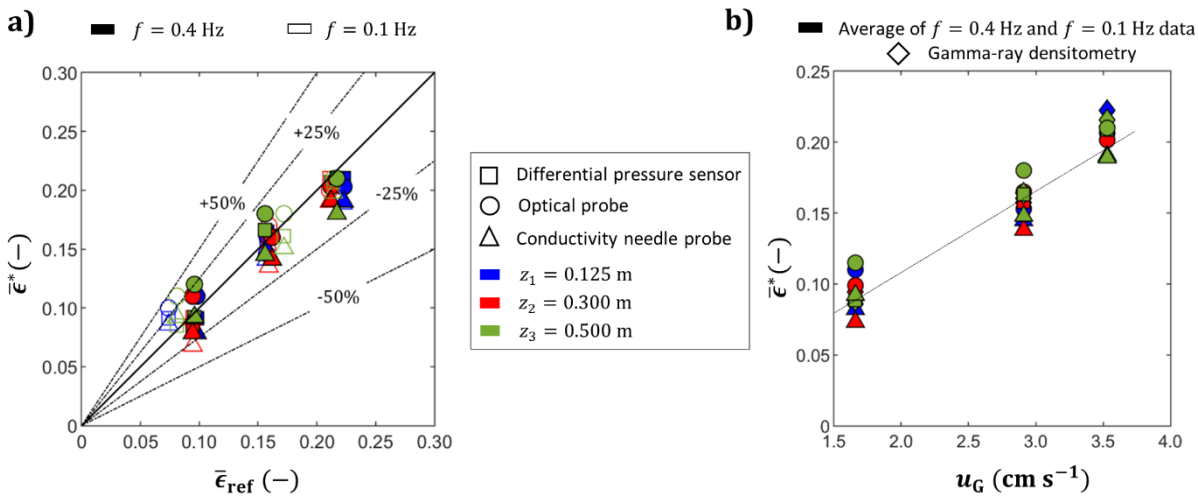

Figure 9. (a) Comparison of measured gas holdup values for the different measurement techniques and planes at different modulation frequencies; (b) measured gas holdup values for the compared measurement techniques.

As shown in **Figures 9a** and **b**, all applied measurement techniques achieve a very good estimate of the average gas holdup. No significant difference between the average holdup values is identified between the three measurement planes. This is reasonable for bubble columns operated in the homogeneous regime (excluding the areas in the vicinity of gas sparger and gas outlet)[13]. This is also an essential requirement for the application of Equations 1 and 2 between two different measurement planes. Based on **Figure 9b**, the average gas holdup increases with the gas superficial velocity, which is also compatible with the homogeneous regime.

4.2 Amplitude damping and phase-shift

For amplitude damping and phase-shift determination, 50% and 10% threshold values were applied for conductivity and optical probes, respectively. For illustrative purposes, the ensemble-averaging procedure was applied for datasets obtained for one exemplary operating point using all the above-mentioned measurement techniques. This allows visualizing the sinusoids contained in the data, which is not directly accessible by the Fourier analysis. The results are reported in **Figure 10**.

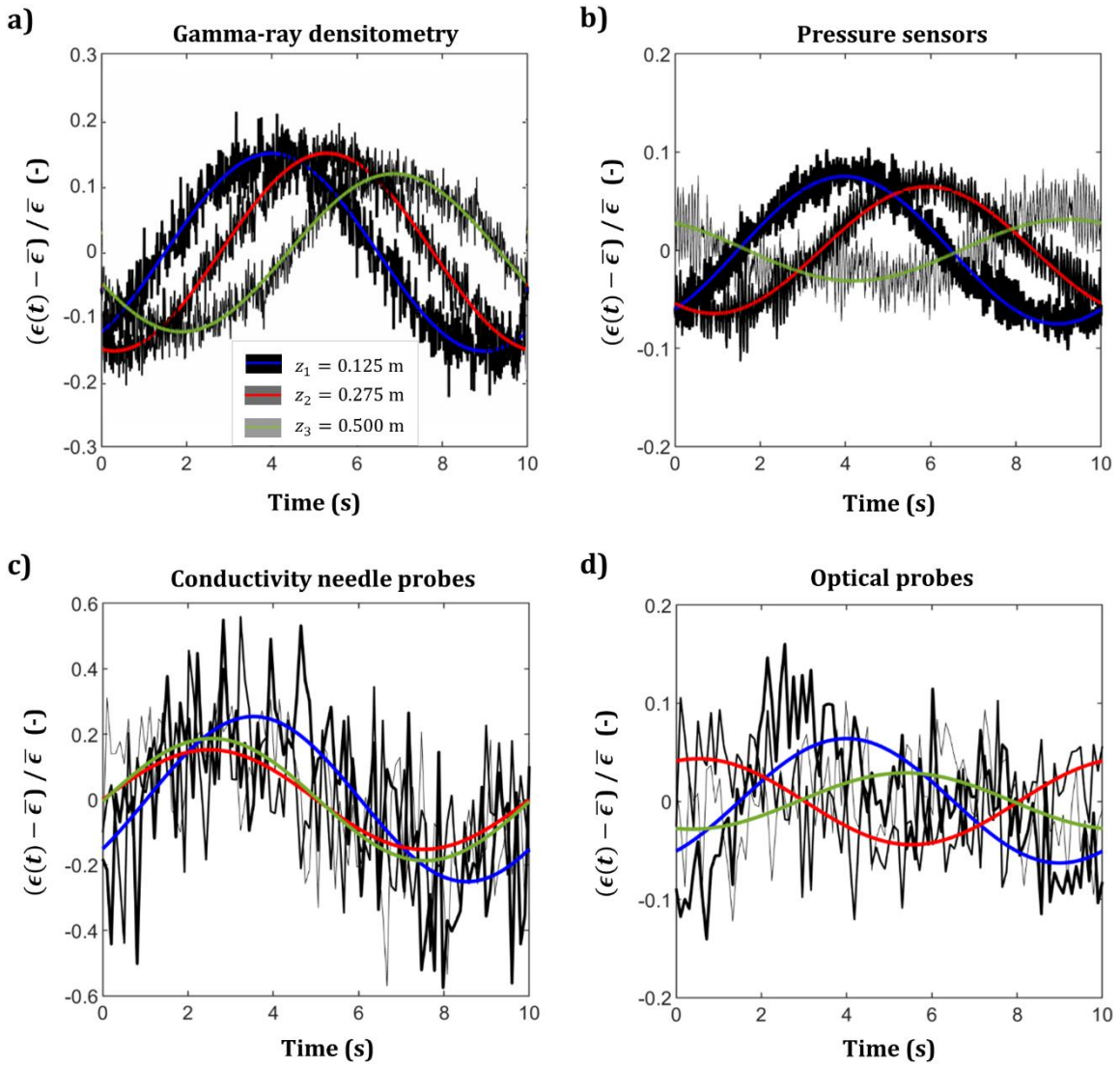

Figure 10. Visualization of the sinusoids obtained applying the ensemble-averaging procedure and least square fitting to the data acquired by (a) gamma-ray densitometry, (b) differential pressure sensors, (c) conductivity needle probes, and (d) optical probes for a gas flow rate of 14 sL min^{-1} and a modulation frequency of 0.1 Hz.

Relatively clear sinusoids can be reconstructed from data of all applied measurement techniques. The amplitude and phase values, however, differ from each other. This results from the limited sensitivity and accuracy of pressure, conductivity and optical sensors with respect to gamma-ray densitometry. In this study, the focus is on amplitude damping and phase-shift, which allow obtaining the axial gas dispersion coefficients.

The results of the performed measurements using non-radiative techniques in terms of amplitude damping (V^*) are reported in **Figure 11**. In the parity plot, obtained values are compared with the results of the gamma-ray densitometry (V_{ref}) for two modulation frequencies and two axial distances (using z_1 as a reference).

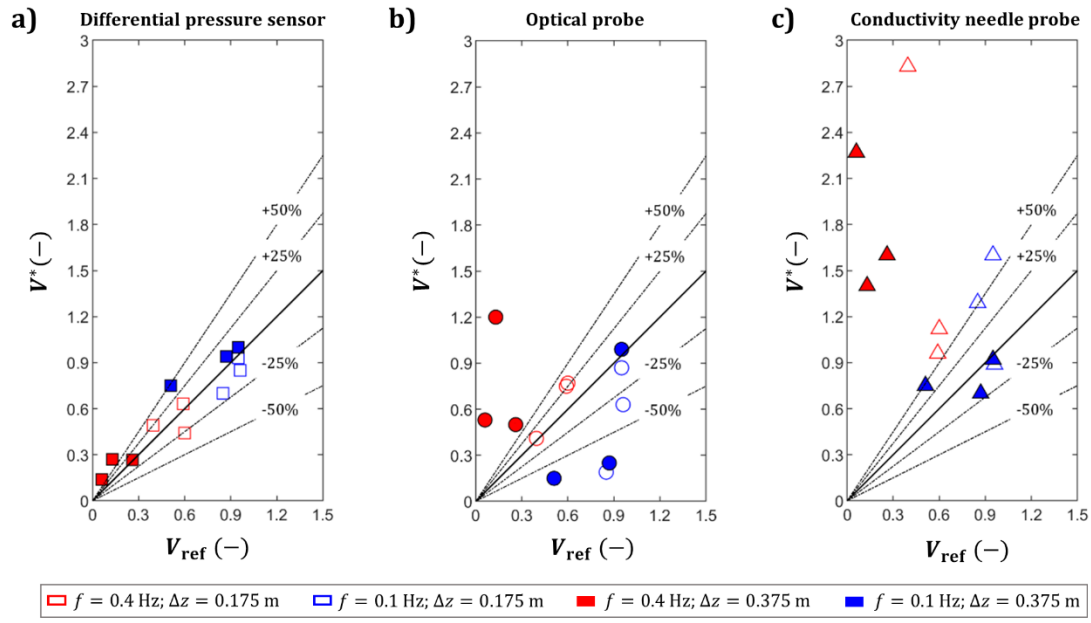

Figure 11. Parity plot of measured amplitude damping (V^*) from (a) differential pressure sensors, (b) optical and (c) conductivity probes compared to values from gamma-ray densitometry (V_{ref}).

Figure 12 is analogous to **Figure 11** and shows the results in terms of phase-shift obtained using pressure, conductivity and optical sensors ($\Delta\phi^*$) in comparison with the phase-shift determined by gamma-ray densitometry ($\Delta\phi_{\mathrm{ref}}$).

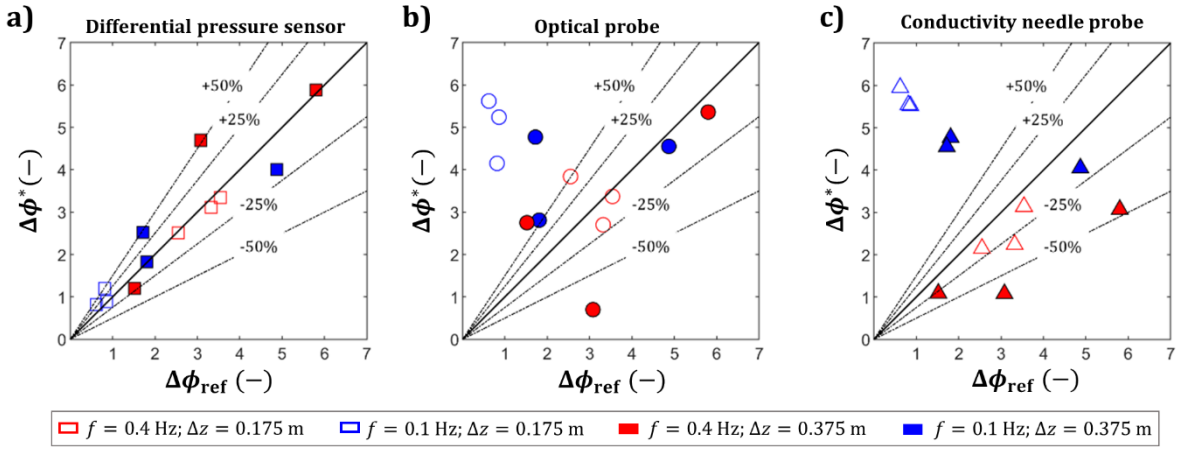

Figure 12. Parity plot of measured phase-shift ($\Delta\phi^*$) from (a) differential pressure sensors, (b) optical and (c) conductivity probes compared to values from gamma-ray densitometry ($\Delta\phi_{\mathrm{ref}}$).

As shown in **Figure 11**, amplitude damping values obtained with conductivity and optical probes show strong deviations (often exceeding $\pm$ 50%). Contrarily, the differential pressure sensors provide reliable values for the amplitude damping (deviations often below $\pm$10%). The higher

deviations at low amplitude damping are caused by the uncertainty of the differential pressure sensors, which plays a bigger role when measuring low amplitude values. **Figure 12** shows that, in general, the phase-shift is more reliably determined than the amplitude damping for the non-radiative techniques. Again, the differential pressure measurements show the best agreement with gamma-ray densitometry. A clear improvement in the performances of all measurement techniques is found for $\Delta z = 0.175$ m and $f = 0.4$ Hz. At these conditions, the gas holdup waves are clearly different from each other in both amplitude and phase. It should be noted that the amplitude of the weakest wave is still sufficiently high to be reliably identified.

4.3 Axial gas dispersion coefficient

For a given column geometry, gas-liquid system and operating conditions, the value of the axial gas dispersion coefficient is unique and independent of the modulation frequency. Marchini et al.[6] pointed out that Equation 1 has more than one solutions, at least in parts of the domain. Thus, results from different modulation frequencies were combined to improve the reliability of the obtained axial gas dispersion coefficients. In this case, the value of the axial gas dispersion coefficients that better fit the obtained measurement results at several axial positions and for different frequencies are taken. Amplitude damping and phase-shifts obtained with optical and conductivity needle probes have been shown in high disagreement with gamma-ray densitometry (see above) and are, therefore, ignored here. **Figure 13** summarizes axial dispersion coefficients obtained by gamma-ray densitometry and differential pressure sensors and show a very good agreement. The axial gas dispersion coefficients are obtained performing a best fit of Equations 1 and 2 to the data reported in **Figures 11a** and **12a**, respectively. The procedure for this fitting is reported by Döß et al.[5].

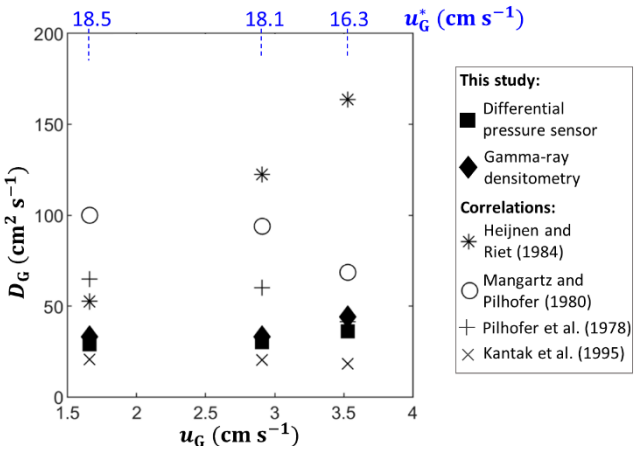

Figure 13. Axial gas dispersion coefficient obtained by gamma-ray densitometry and differential pressure sensors and comparison with literature correlations.

Predictions from correlations available in the literature are also given in **Figure 13**. Döß et al.[5] comprehensively reviewed the correlations available in the literature for predicting the axial gas dispersion coefficient and the conditions at which they were derived. In the current study, only correlations derived for columns with ID<150 mm and $u_G <$ 18 cm s^{-1} were considered. The general form of all the applied correlations is

$$D_G = C_1 D_c^{j_1} \cdot C_2 u_G^{j_2} \cdot C_3 u_G^{*\,j_3}, \qquad 21$$

where D_c is the column diameter. The values of the parameters for the different correlations are reported in **Table 2**. The bubble rise velocity (u_G^*) was assumed equal to the bubble swarm velocity and estimated as $u_G/\bar{\epsilon}$.

Table 2. References and parameters of Equation 21 for correlations used in **Figure 13**.

Reference	C_1	j_1	C_2	j_2	C_3	j_3
Heijnen and Riet[14]	78	1.5	1.0	1.5	-	-
Mangartz and Pilhofer[15]	50	1.5	-	-	1	3
Pilhofer et al.[16]	-	-	-	-	2.64	3.56
Kantak et al.[17]	0.2	1.25	-	-	1	1

Figure 14 shows that the correlation of Heijnen and Riet[14] (the only one based on the gas superficial velocity) strongly overpredicts the obtained values of the axial gas dispersion coefficient, especially at higher flow rates. This might be due to the fact that in the case of a perforated plate with relatively high free fractional area (as the one used in the current study) not all gas injection holes are active at the same time. This is especially true at low gas flow rates. In this case, increasing gas flow rates lead to an increased number of active holes (and therefore more bubbles detaching at the same time), while the bubble rise velocity remains almost constant, as shown in **Figure 14** (changes are less than 10%). Thus, the bubble rise velocity should be considered as a characteristic parameter for the column. In fact, correlations based on the bubble rise velocity show a better agreement with the data obtained in this study. In particular, the correlations from Kantak et al.[17] are in good agreement.

Correlations from Mangartz and Pilhofer [15], Pilhofer et al.[16] and Kantak et al.[17] all predict a slightly decreasing trend that is due to a slight decrease in the bubble rise velocity in the current study. The same trend is not directly visible in the data from this study. It should be considered, however, that, for applying the correlations, the bubble rise velocity was estimated as $u_G/\bar{\epsilon}$, as mentioned above. Both u_G and $\bar{\epsilon}$ are measured values and subjected to experimental uncertainties. Their ratio is, most likely, subjected to higher uncertainty than a directly measurement of the bubble rise velocity. Therefore, this slight inconsistency should be disregarded.

5. Conclusion and future work

This study evaluates the possibility of substituting gamma-ray densitometry for measuring the axial gas dispersion coefficient in bubble columns via GFM by a non-radiative measurement technique. In particular, differential pressure sensors, conductivity needle probes and transmittance optical sensors were considered. A satisfactory value of the average gas holdup and a rather clear sinusoidal wave could be obtained from the dataset of all applied measurement techniques. However, amplitude damping and phase-shifts obtained by conductivity and transmittance-based sensors were not at all in agreement with gamma-ray densitometry results. This is mostly due to the local measurements of both probes and to the difficulty of selecting an appropriate threshold for data processing. In addition, measurements are intrusive and highly local. Local measurements might not be representative of the holdup value on the column cross-section. In fact, local hydrodynamic characteristics (such as the presence of stagnant areas and recirculation paths on a small scale) strongly affect the results. A local sinusoidal wave is, therefore, measured but its amplitude and phase do not necessarily correspond to the ones average holdup wave. As a consequence, conductivity needle probes and transmittance optical sensors cannot be recommended for the GFM. Contrarily, differential pressure sensors showed excellent reliability in identifying amplitude damping and phase-shift. The results were well reproducible. The differential pressure sensor measurements are affected by holdup values of the entire column cross-section. Similarly, gamma-ray densitometry measurements account for holdup values in a full chord of the column cross-section. Mainly thanks to this similarity, a good agreement is obtained. The values of the axial gas dispersion coefficient obtained by differential pressure sensors and gamma-ray densitometry showed a very good agreement with deviations between 5 and 15%. A reasonable agreement with the predictions of available correlations was also achieved.

Based on the data collected in this study, differential pressure sensors are a viable alternative to gamma-ray densitometry in GFM, provided that high-accuracy low-range sensors are applied. Differential pressure sensors are a readily available and cost-efficient measurement technique. They can be installed at several measurement planes, where data can be acquired simultaneously, drastically reducing the time needed for collecting a complete dataset. This will massively simplify the application of GFM in industrial environments, where gamma-ray densitometry might be not available or pose safety concerns. In the future, differential pressure sensors might also prove particularly advantageous in large columns, were the statistics of the photon counting process would require prohibitively long scanning times for gamma-ray densitometry.

Marchini et al.[6] comprehensively investigated the sensitivity of the determined axial gas dispersion coefficient to deviations in the measured amplitude damping and phase-shift. The authors proved that the sensitivity strongly depends on the values of the axial gas dispersion coefficient itself, on the axial distance between the measurement points and on the applied modulation frequency. Therefore, it is possible to optimize the modulation parameters based on a first approximation of the axial gas dispersion coefficient to reduce the uncertainty in the next experiments. Practically, this is feasible only if single experiments can be performed at reasonable costs, as in the case of differential pressure sensors. In this way, multiple repetitions of the same experiments can also be easily performed to check for data reproducibility.

In the future, GFM based on differential pressure sensors will allow for extensive characterization of axial gas dispersion in bubble columns and the development of new correlations.

6. Supporting Information

This information is available free of charge via the Internet at http://pubs.acs.org/.

7. Acknowledgement

This work was supported by the German Research Foundation (DFG), (HA 3088/18-1).

Nomenclature

Symbol	Description	Unit
$A_{\epsilon,0}$	Initial modulation amplitude	
A_{ϵ}	Amplitude of the gas holdup wave	
D_{C}	Column diameter	m
D_{G}	Axial gas dispersion coefficient	$\mathrm{m^2 s^{-1}}$

f	Modulation frequency	Hz
f_{d}	Sampling frequency	Hz
g	Gravitational acceleration	$\mathrm{m\ s^{-2}}$
H_1	Parameter used in Section 4.1 $H_1 = \frac{u_{\mathrm{G}}^*}{2D_{\mathrm{G}}}$	$\mathrm{m^{-1}}$
H_2	Parameter used in Section 4.1 $H_2 = \sqrt{1 + \frac{16\omega^2 D_{\mathrm{G}}^2}{u_{\mathrm{G}}^{*\,4}}}$.	
K_1	Parameter used in Section 4.1 $K_1 = K_1\left[1 - \frac{\sqrt{1+K_2}}{\sqrt{2}}\right]$	$\mathrm{m^{-1}}$
K_2	Parameter used in Section 4.1 $K_2 = \frac{K_1\sqrt{K_2-1}}{\sqrt{2}}$.	$\mathrm{m^{-1}}$
l	Object's penetration length	m
N	Expected number of photons counted by the detector with the object in place	cps
N_0	Expected number of photons exiting the source without the object in place	cps
n	Scanning interval	
n_{p}	Total number of modulation periods	
n_{s}	Total number of scanning intervals	
P	Pressure	Pa
t	Time	s
u_{G}	Gas superficial velocity	$\mathrm{ms^{-1}}$
u_{G}^*	Bubble rise velocity	$\mathrm{ms^{-1}}$
V	Amplitude damping between two axial positions	
V^*	Amplitude damping between two axial positions measured with non-radiative measurement techniques	
V_{ref}	Amplitude damping between two axial positions measured with gamma-ray densitometry	
z	Axial distance from the sparger	m
Δz	Axial distance between two measurement planes	m

Greek letters

μ	Attenuation coefficient	$\mathrm{m^{-1}}$
ϵ	Gas holdup	
$\bar{\epsilon}$	Average gas holdup	

$\tilde{\epsilon}$	Ensemble-averaged gas holdup wave	
$\bar{\epsilon}^*$	Average gas holdup obtained with non-radiative measurement techniques	
$\bar{\epsilon}_{\mathrm{ref}}$	Average gas holdup obtained with gamma-ray densitometry	
ρ	Density	kg m^3
ϕ	Phase of the gas holdup wave	rad
ϕ_0	Initial phase of the gas holdup wave	rad
$\Delta\phi$	Phase-shift of the gas holdup wave	rad
$\Delta\phi^*$	Phase-shift of the gas holdup wave measured with non-radiative measurement techniques	rad
$\Delta\phi_{\mathrm{ref}}$	Phase-shift of the gas holdup wave measured with gamma-ray densitometry	rad
ω	Angular modulation frequency	rad s^{-1}

Subscripts

k, i	Indexes
G	Gas phase
L	Liquid phase
GL	Mixture of gas and liquid phases

References

1. Hampel, U. Anordnung und Verfahren zur Dispersionsmessung sowie Mehrphasenapparat mit einer solchen Anordnung. Patent DE 10 2014 118 649 B3 2015.12.24. 2015.
2. Deckwer, W.-D., *Bubble column reactors*. Wiley New York, 1992; Vol. 200.
3. Kantak, M. V.; Hesketh, R. P.; Kelkar, B. G., Effect of Gas and Liquid Properties on Gas-Phase Dispersion in Bubble-Columns. *Chem Eng J Bioch Eng* **1995,** *59* (2), 91-100.
4. Demaria, F.; White, R. R., Transient Response Study of Gas Flowing through Irrigated Packing. *Aiche Journal* **1960,** *6* (3), 473-481.
5. Döß, A.; Schubert, M.; Bieberle, A.; Hampel, U., Non-invasive determination of gas phase dispersion coefficients in bubble columns using periodic gas flow modulation. *Chemical Engineering Science* **2017,** *171*, 256-270.
6. Marchini, S.; Schubert, M.; Hampel, U., Analysis of the effect of uncertainties in hydrodynamic parameters on the accuracy of the gas flow modulation technique for bubble columns. *Chemical Engineering Jornal* **2022,** *434*.
7. Viswanathan, M.; Mathuranathan, V., Digital Modulations using MATLAB. *Building Simulation Models from Scratch. India, Pilani* **2017**.
8. Munholand, L.; Soucy, G., Comparison of four conductive needle probe designs for determination of bubble velocity and local gas holdup. *Review of scientific instruments* **2005,** *76* (9), 095101.
9. Dias, S. G.; França, F. A.; Rosa, E. S., Statistical method to calculate local interfacial variables in two-phase bubbly flows using intrusive crossing probes. *International Journal of Multiphase Flow* **2000,** *26* (11), 1797-1830.

10. Schweitzer, J. M.; Bayle, J.; Gauthier, T., Local gas hold-up measurements in fluidized bed and slurry bubble column. *Chemical Engineering Science* **2001,** *56* (3), 1103-1110.
11. Xuereb, C.; Riba, J.-P., A double optical-fiber probe to characterize gas-phase properties in gas-liquid contactors. *Sensors and Actuators A: Physical* **1995,** *47* (1), 349-352.
12. Coté, G. L.; Wang, L. V.; Rastegar, S., Chapter 17 - Biomedical Optics and Lasers. In *Introduction to Biomedical Engineering (Third Edition)*, Enderle, J. D.; Bronzino, J. D., Eds. Academic Press: Boston, 2012; pp 1111-1173.
13. Jin, H.; Yang, S.; Guo, Z.; He, G.; Tong, Z., The axial distribution of holdups in an industrial-scale bubble column with evaluated pressure using γ-ray attenuation approach. *Chemical Engineering Journal* **2005,** *115* (1-2), 45-50.
14. Heijnen, J.; Van't Riet, K., Mass transfer, mixing and heat transfer phenomena in low viscosity bubble column reactors. *The Chemical Engineering Journal* **1984,** *28* (2), B21-B42.
15. Mangartz, K.; Pilhofer, T., Untersuchungen zur Gasphasendispersion in Blasensäulenreaktoren. *Verfahrenstechnik* **1980,** *14*, 40.
16. Pilhofer, T.; Bach, H.; Mangartz, K., Determination of fluid dynamic parameters in bubble column design. *ACS Symposium Series* **1978,** *65*, 372-383.
17. Kantak, M.; Hesketh, R.; Kelkar, B., Effect of gas and liquid properties on gas phase dispersion in bubble columns. *The Chemical Engineering Journal and The Biochemical Engineering Journal* **1995,** *59* (2), 91-100.

Table of Content Graphic